Low-field switching of noncollinear spin texture at $La_{0.7}Sr_{0.3}MnO_3$-$SrRuO_3$ interfaces

S. Das,[1,2,*] A. D. Rata,[1] I. V. Maznichenko,[1] S. Agrestini,[3] E. Pippel,[4] N. Gauquelin,[5] J. Verbeeck,[5] K. Chen,[6] S. M. Valvidares,[7] H. Babu Vasili,[7] J. Herrero-Martin,[7] E. Pellegrin,[7] K. Nenkov,[2] A. Herklotz,[1] A. Ernst,[4] I. Mertig,[1,4] Z. Hu,[3] and K. Dörr[1,2,†]

[1]*Institute of Physics, Martin Luther University Halle-Wittenberg, 06099 Halle, Germany*
[2]*IFW Dresden, Institute for Metallic Materials, Postfach 270116, 01171 Dresden, Germany*
[3]*Max Planck Institute for Chemical Physics of Solids, Nöthnitzer Strasse 40, 01187 Dresden, Germany*
[4]*Max Planck Institute of Microstructure Physics, Weinberg 2, 06120 Halle, Germany*
[5]*EMAT, University of Antwerp, Groenenborgerlaan 171, 2020 Antwerp, Belgium*
[6]*Institute of Physics II, University of Cologne, Zülpicher Strasse 77, 50937 Cologne, Germany*
[7]*ALBA Synchrotron Light Source, E-08290 Cerdanyola del Vallès, Barcelona, Spain*

(Received 24 June 2018; revised manuscript received 4 November 2018; published 15 January 2019)

Interfaces of ferroic oxides can show complex magnetic textures which have strong impact on spintronics devices. This has been demonstrated recently for interfaces with insulating antiferromagnets such as $BiFeO_3$. Here, noncollinear spin textures which can be switched in very low magnetic field are reported for conducting ferromagnetic bilayers of $La_{0.7}Sr_{0.3}MnO_3$-$SrRuO_3$ (LSMO-SRO). The magnetic order and switching are fundamentally different for bilayers coherently grown in reversed stacking sequence. The SRO top layer forms a persistent exchange spring which is antiferromagnetically coupled to LSMO and drives switching in low fields of a few milliteslas. Density functional theory reveals the crucial impact of the interface termination on the strength of Mn-Ru exchange coupling across the interface. The observation of an exchange spring agrees with ultrastrong coupling for the MnO_2/SrO termination. Our results demonstrate low-field switching of noncollinear spin textures at an interface between conducting oxides, opening a pathway for manipulating and utilizing electron transport phenomena in controlled spin textures at oxide interfaces.

DOI: 10.1103/PhysRevB.99.024416

I. INTRODUCTION

Coupling of magnetic layers across interfaces in thin-film heterostructures is a key property for magnetic sensors, spintronics, and data storage devices. Both exchange and Dzyaloshinskii Moriya (DM) interactions can alter the magnetic order at interfaces. As a consequence, various functional properties of magnetic interfaces can be controlled through engineering magnetic interfacial interactions. This kind of approach is often utilized for interfaces in thin-film heterostructures of metals and alloys [1,2], while it is yet little exploited for complex oxides. Recent examples are the selection of electronic spin polarization in tunnel junctions with a $LaFeO_3$ barrier [3,4] and the impact of interfacial magnetism on the exchange bias exerted by magnetoelectric $BiFeO_3$ [5–7]. For both interface types, an insulating antiferromagnet ($LaFeO_3$, $BiFeO_3$) shows induced in-plane magnetization at the interface to a ferromagnet ($La_{0.7}Sr_{0.3}MnO_3$). On the other hand, strong DM interaction has been suggested for the $SrRuO_3$/$SrIrO_3$ interface where the heavy Ir ion induces substantial spin-orbit coupling, resulting in the observation of an (electrically tunable) topological Hall effect (THE) attributed to the formation of noncoplanar interfacial spin textures [8,9]. The magnetocrystalline anisotropy, the other vital parameter governing spin textures, has been revealed to depend on the coherent rotations of oxygen octahedrons at interfaces of ABO_3-perovskite-type magnetic oxides (with metals A, B) [10–16]. In general, it is yet rarely known or predictable, which magnetic textures arise at coherent oxide interfaces and how they can be systematically controlled. Here, we present an investigation on interfaces between two prototype conducting ferromagnets, $SrRuO_3$ and $La_{0.7}Sr_{0.3}MnO_3$, which are often used in device heterostructures. Noncollinear interfacial magnetism is found to appear in distinctly different forms depending on the growth sequence of the layers, profoundly changing magnetic switching and the resulting exchange-bias characteristics. The $La_{0.7}Sr_{0.3}MnO_3$/$SrRuO_3$ (LSMO/SRO) interface [17–27] has been a focus of interest for some years because of the unusually large interfacial antiferromagnetic coupling. Originally, Ke *et al.* reported on an exchange-bias effect in bilayers of the soft ferromagnet LSMO and the hard ferromagnet SRO [17]. Very large exchange-bias fields of several teslas and low-temperature magnetization loops of peculiar shape were found for coherent superlattices of $[SRO/LSMO]_n$/STO(001) with layer thicknesses of a few unit cells and interfaces showing very low interdiffusion [18,20–22]. In such superlattices, a depth-dependent magnetization reorientation in SRO near the interface with LSMO was detected in neutron depolarization measurements and the presence of an exchange spring has been suggested [24]. We investigate the element-specific magnetic switching employing x-ray magnetic circular dichroism (XMCD)

*sujitdask@gmail.com
†kathrin.doerr@physik.uni-halle.de

measurements [19,28,29] in bilayers to gain a clearer understanding of element-specific magnetic order. We analyze the magnetic hysteresis of Mn and Ru moments derived from field-dependent XMCD spectra of LSMO-SRO bilayers grown coherently on $SrTiO_3(001)$ in either sequence. Magnetic switching and remanent interfacial magnetic textures are distinctly different for both cases and feature noncollinear spin orders of either Ru or Mn, respectively. Strikingly, for the SRO top layer, SRO as hard-magnetic bulk material is found to form a persistent exchange spring switchable in low magnetic field of a few milliteslas (mT). Results from density functional theory indicate strongly different magnitudes of Mn-Ru interfacial exchange coupling for the two chemical interface terminations. The appearance of the exchange spring is in agreement with the case of stronger coupling for the MnO_2/SrO termination. Additionally, the interfacial magnetic anisotropy of both top layers in the bilayers is altered, contributing to the formation of the noncollinear interfacial spin textures.

II. EXPERIMENT

$La_{0.7}Sr_{0.3}MnO_3$ (LSMO) and $SrRuO_3$ (SRO) layers have been grown on $SrTiO_3(001)$ substrates by pulsed laser deposition (PLD) using an excimer laser with a 248-nm wavelength and a PLD chamber (Surface GmbH) with high-pressure reflection high-energy electron diffraction (RHEED) facility. The single-crystalline $SrTiO_3$ (STO) substrates were terminated with TiO_2. The growth temperature, laser energy density, and oxygen pressure were 700 °C, 0.3 J/cm^2, and 0.2 mbar, respectively. After growth, samples were annealed for 1 h in oxygen of 200 mbar. (More details on sample growth are described in the Supplemental Material [30]; also see Refs. [31,32].) Coherent growth of both layers, LSMO and SRO, on STO(001) with an in-plane lattice parameter of $a = 3.905$ Å has been confirmed by x-ray diffraction and high-resolution scanning transmission electron microscopy (STEM). STEM using high-angle annular dark field (HAADF) Z contrast and electron energy loss spectroscopy (EELS) have been applied to analyze the atomic interface structure. The XMCD experiments were performed at the BL29 BOREAS beamline at the ALBA synchrotron radiation facility. The x-ray absorption was measured using circular polarized light with the photon spin parallel (σ^+) or antiparallel (σ^-) with respect to the magnetic field. The spectra were collected with the beam in grazing incidence (20° to the film surface and with $H \parallel$ to the incoming x-ray beam) and in normal incidence (x-ray beam and $H \perp$ film surface) [28]. The degree of circular polarization delivered by the Apple II–type elliptical undulator was 70% for the Ru L edge and close to 100% for the Mn L edge. The spectra were recorded using the total electron yield method (by measuring the sample drain current) in a chamber with a vacuum base pressure of 2×10^{-10} mbar. The XMCD data were measured at $T = 60$ K after cooling the samples in a field of 3 T. The Ru-XMCD hysteresis loops were obtained by measuring the Ru L_3 edge XMCD spectrum for each value of magnetic field and integrating the XMCD signal. The Mn-XMCD hysteresis loops were obtained by measuring, as a function of applied field, the Mn L_3 edge XMCD signal at the energy where the XMCD signal is maximum. Magnetization measurements were conducted in a superconducting quantum interference device (SQUID) magnetometer.

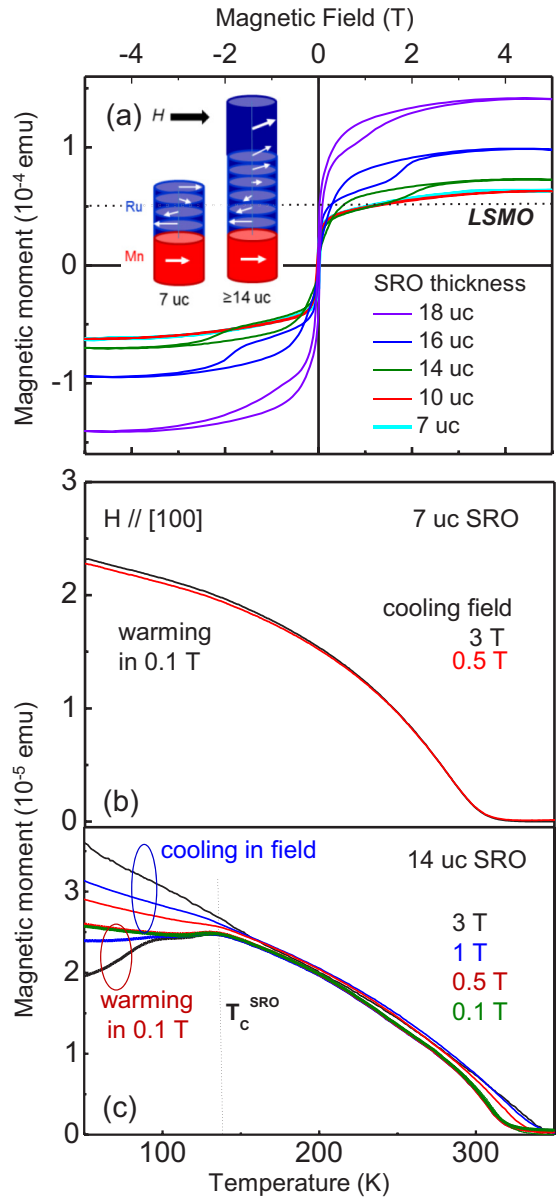

FIG. 1. Magnetization of SRO/LSMO/STO(001) bilayers with varied SRO layer thickness (7 – 18 unit cells). (a) Field-dependent hysteresis at 20 K in magnetic field $H \parallel [100]$. The dashed line marks the nominal LSMO magnetization derived from 3.7 μ_B/Mn. Inset: Schematic spin orientations in an in-plane field. Note the Ru spin out-of-plane canting with growing SRO thickness. (b), (c) Temperature-dependent magnetization of two bilayer samples measured during warming in 0.1 T after cooling in different cooling fields. In (c), the magnetization during cooling is also shown.

III. RESULTS AND DISCUSSION

A. Magnetization

Figure 1(a) shows in-plane magnetization loops measured at 10 K, $H \parallel [100]$ of bilayer samples with 9-uc LSMO

bottom layer (uc denoting pseudocubic unit cells) and varied SRO top layer thickness of $d_{SRO} = 7$–18 uc. In order to highlight the effect of increasing SRO thickness, the total magnetic moment is plotted and compared to the value expected for collinear LSMO [dashed line in Fig. 1(a)]. For 7 and 10 uc of SRO, the magnetization loops are free of hysteresis and show no saturation up to 5 T. The magnetic moment is below that of a single LSMO layer at 0.5 T and larger than that at 5 T, reflecting a gradual reversible rotation of Ru spins in the field [as depicted in the inset of Fig. 1(a)]. Note that a breaking of the antiferromagnetic Mn-Ru interfacial coupling would reveal itself as a transition associated with irreversibility. Hence, the magnetic moment of Ru appears to be rigidly coupled to the Mn moment at the interface in magnetic fields below 5 T. This behavior is characteristic of the field-induced reversible rotation in an exchange spring [33–35]. Upon increasing the SRO thickness, a hysteretic transition appears in all bilayers with $d_{SRO} \geqslant 14$ uc [Fig. 1(a)]. With increasing d_{SRO}, the transition field decreases from ~2 T to lower values. This is in agreement with field-driven reversal of an upper part of the SRO which is exchange coupled to the fixed interfacial SRO layer. (The transition does *not* result from reversing the magnetization of the complete SRO film—an interpretation found in all previous studies where collinear SRO magnetic order was assumed.) Hence, an interfacial SRO layer of about 10 uc thickness seems to form an exchange spring pinned to the adjacent LSMO layer. Thicker SRO contains an exchange spring layer (ESL) and a part about 10 uc away from the interface which appears to behave similarly to coherently strained SRO on STO(001) and is exchange coupled to the ESL. This interpretation is consistent with the temperature-dependent magnetization measured during warming in 0.1 T after field cooling in different fields [Figs. 1(b) and 1(c)]. The bilayer with 7-uc SRO has even no detectable anomaly at the Curie temperature of SRO (not far from bulk $T_C^{SRO} \sim$ 150 K), suggesting that the order of Ru magnetic moments

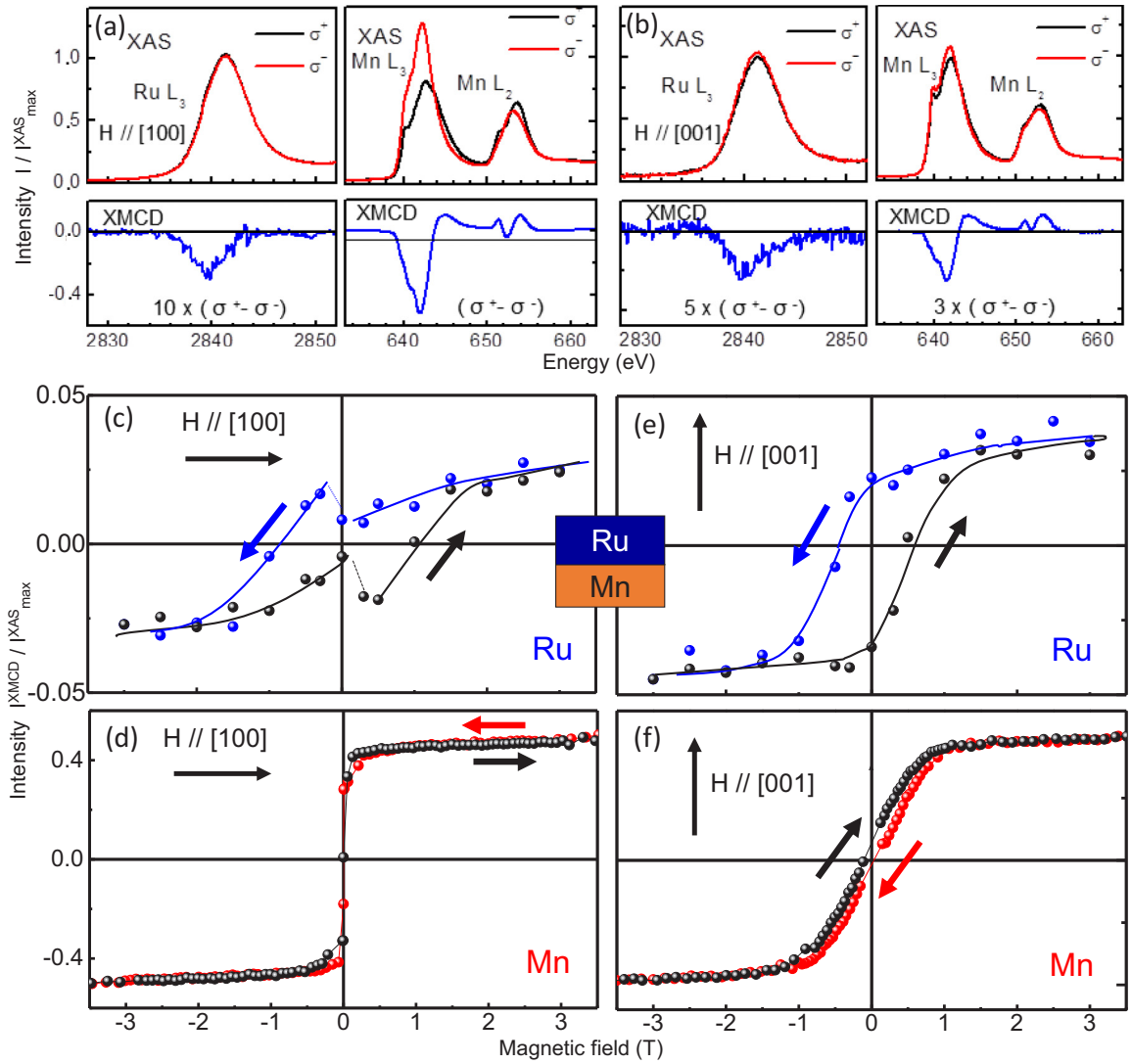

FIG. 2. Element-resolved magnetic hysteresis of a $SrRuO_3$(14 uc)/$La_{0.7}Sr_{0.3}MnO_3$(9uc)/$SrTiO_3$(001) bilayer. X-ray absorption spectra at the Ru L_3 and the Mn $L_{2,3}$ edges in grazing incidence (a) and normal incidence (b) configurations recorded at 60 K in 0.2 T. Ru in-plane (c) and out-of-plane (e) hysteresis loops and Mn in-plane (d) and out-of-plane (f) hysteresis loops. Intensities are normalized to the maximum absorption value I_{max}^{XAS} (averaged over both polarizations).

appears or vanishes gradually with temperature. In contrast, a distinct anomaly at T_C^{SRO} and a peculiar field-cooling effect is observed for $d_{SRO} = 14$–18 uc [Fig. 1(c), for 14 uc]. A larger cooling field causes *smaller* total magnetization after removal of the field at 20 K. Based on the exchange-spring model, this can be understood as follows. The magnetocrystalline anisotropy of SRO at 20 K is large enough to pin the top part of the SRO layer in the positive field direction. The Ru exchange spring relaxes itself by reversing the soft-magnetic LSMO layer after removal of the field, leading to the observed drop of magnetization. The efficiency of this process depends on the fraction of the SRO top part that was aligned in the cooling field.

B. XMCD

The element-specific magnetic switching of a sample with a 14-uc SRO top layer and a 9-uc LSMO bottom layer has been investigated by measuring field-dependent x-ray magnetic circular dichroism (XMCD) at the Mn $L_{2,3}$ and Ru $L_{2,3}$ edges with a monochromatic photon beam at grazing incidence (in-plane component $H \| [100]$) or normal incidence ($H \| [001]$, out of plane). Figure 2 presents in-plane and out-of-plane Mn and Ru magnetic hysteresis loops. Most strikingly, LSMO shows pronounced soft-magnetic reversal of Mn moments in the plane of the film with a coercive field of $\leqslant 10$ mT [Fig. 2(d); we note that the resolution of magnetic fields below 10 mT is not accurate]. This resembles the behavior of single LSMO/STO(001) films with in-plane easy axes [36,37]; however, LSMO is strongly coupled to SRO here. In the framework of the exchange-spring model, the easy reversal of LSMO (and the connected Ru ESL) is rather natural, since the Ru exchange spring relaxes after removal of an applied field, reversing the rigidly coupled LSMO layer. Before addressing the Ru hysteresis loops, we recall the characteristics of SRO/STO(001) single-layer films: Ferromagnetic loops with large remanence are obtained in plane and out of plane due to a strong canting of the Ru moments [28,38]. In the bilayer, the in-plane Ru loop

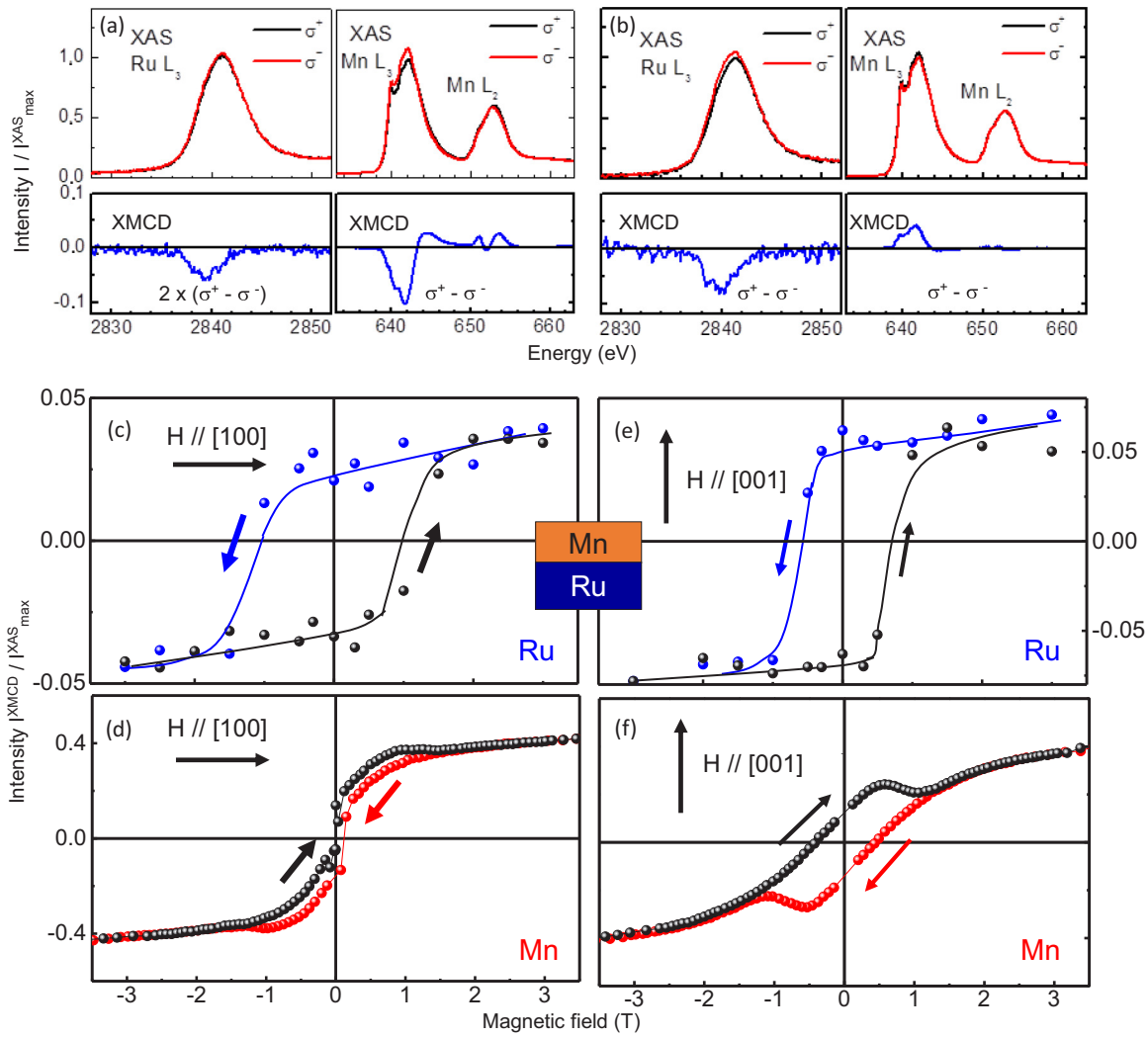

FIG. 3. Magnetic hysteresis loops at 60 K of the $La_{0.7}Sr_{0.3}MnO_3$(9 uc)/$SrRuO_3$(14 uc)/$SrTiO_3$(001) bilayer. X-ray absorption spectra at the Ru L_3 and the Mn $L_{2,3}$ edges in grazing incidence (a) and normal incidence (b) configurations recorded at 60 K in 0.2 T. Ru in-plane (c) and out-of-plane (e) hysteresis loops and Mn in-plane (d) and out-of-plane (f) hysteresis loops. Intensities are normalized to the maximum absorption value I_{max}^{XAS} (averaged over both polarizations).

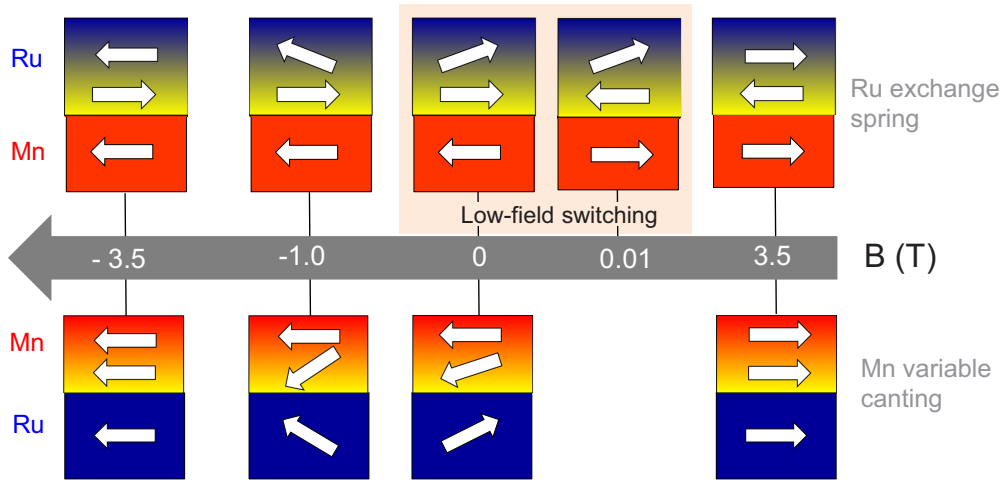

FIG. 4. Noncollinear magnetic order in the LSMO-SRO bilayers during the sweeping of an in-plane magnetic field ($H \| [100]$) from large positive to negative values. Switching fields at 60 K taken from Figs. 2 and 3. Arrows indicate spin orientations, with graded color marking a gradual spin rotation. Note the stable antiferromagnetic Mn-Ru interfacial coupling in the case of Ru exchange spring. Ru spins are canted out of plane like in single films on STO(001), apart from the interface region in the upper panel.

[Fig. 2(c)] exhibits a peculiar shape: Starting at the positive maximum value at 3.5 T, a gradual decrease appears during the decrease of the field, followed by an *increase* when the magnetic field turns negative. In the framework of the exchange-spring model, this loop shape naturally results from interfacial Ru moments rigidly coupled antiparallel to Mn moments. Switching the Mn moments to the negative orientation brings the interfacial Ru moments back to positive orientation in a very small field, while the top part of the SRO aligns only when a larger field of $\sim$1 T is applied. The corresponding Mn out-of-plane hysteresis loop [Fig. 2(f)] has a very small remanence; hence, the out-of-plane canting of Mn moments is negligible. Based on the strong 180° antiferromagnetic Mn-Ru coupling, this reveals an in-plane orientation of Ru spins directly at the interface. The reversed character of the out-of-plane Mn hysteresis loop is a consequence of the antiferromagnetic exchange coupling to the SRO layer. The Ru out-of-plane hysteresis loop [Fig. 2(e)] is nearly rectangular with large remanence, revealing substantial out-of-plane canting of the SRO top part. The element-resolved magnetic switching data confirm that the magnetic structure of the 14-uc-thick SRO top layer is not collinear ferromagnetism, and instead agree with the suggested exchange-spring model.

A fundamentally different behavior is found if layers are coherently grown in the reversed sequence of LSMO/SRO/STO(001), keeping all other parameters fixed. Figure 3 presents XMCD data like those of Fig. 2 for the reversed-layer sample type. Here, the Ru in-plane [Fig. 3(c)] and out-of-plane [Fig. 3(e)] magnetization loops are typical ferromagnetic ones with a large remanence, indicating canted out-of-plane orientation of Ru moments. Besides the larger coercive fields attributed to the antiferromagnetic interfacial coupling to LSMO, the Ru switching is consistent with previous magnetization [38] and XMCD [28] data of single-layer coherently grown SRO/STO(001) films. The Mn in-plane hysteresis loop [Fig. 3(d)] has an inverted character; i.e., it shows negative remanence after application of +3.5 T. This reflects the antiferromagnetic Mn-Ru interface coupling, since Ru moments have positive remanence and drive Mn moments to the negative in-plane direction at zero field. More strikingly, the out-of-plane Mn hysteresis [Fig. 3(f)] has substantial remanence, revealing an out-of-plane canting of Mn moments. Single coherently strained LSMO/STO(001) films have magnetic in-plane easy axes [36,37]. Hence, the magnetic anisotropy of the LSMO layer has been altered in this sample type as a consequence of interfacial coupling to SRO. It is likely that far from the interface the magnetic anisotropy of LSMO is identical to coherently strained single-layer LSMO/STO(001). Thus, Mn spins experience a disturbance of the collinear ferromagnetic order at this type of LSMO-SRO interface. Note that the XMCD intensity of Mn comes close to the same saturated value of 40%–45% in a large field in Figs. 2 and 3, reflecting the restoration of the collinear ferromagnetic order of Mn moments in large fields. There is a weak (stronger) dip of the Mn-XMCD signal in Fig. 3(d) [Fig. 3(f)] where Ru spins are switched. This indicates a slight canting away of Mn spins from the field direction due to the antiferromagnetic coupling with Ru spins. We find no evidence for a Mn ESL in this bilayer type: The XMCD results can be accounted for considering a variable canting of Mn moments. Interestingly, both bilayer cases have in common that the interfacial magnetic anisotropy of the *top* layer is distinctly different from that of a coherently strained single film (further discussed below).

The magnetic structure of the LSMO-SRO bilayers in a magnetic field applied in plane ($H \| [100]$) and swept from +3.5 T to –3.5 T is schematically summarized in Fig. 4. In case of the SRO top layer, a Ru exchange spring is formed. Antiferromagnetic interfacial coupling is stable in the applied field range. Hence, switching occurs inside the Ru exchange-spring layer (ESL). At remanence, the exchange spring is relaxed, and the relaxation happens in a very small field ($\leqslant$10 mT). In the case of the LSMO top layer, Mn shows variable canting at the interface, dependent on the orientation of Ru spins. Antiferromagnetic interfacial coupling is weaker

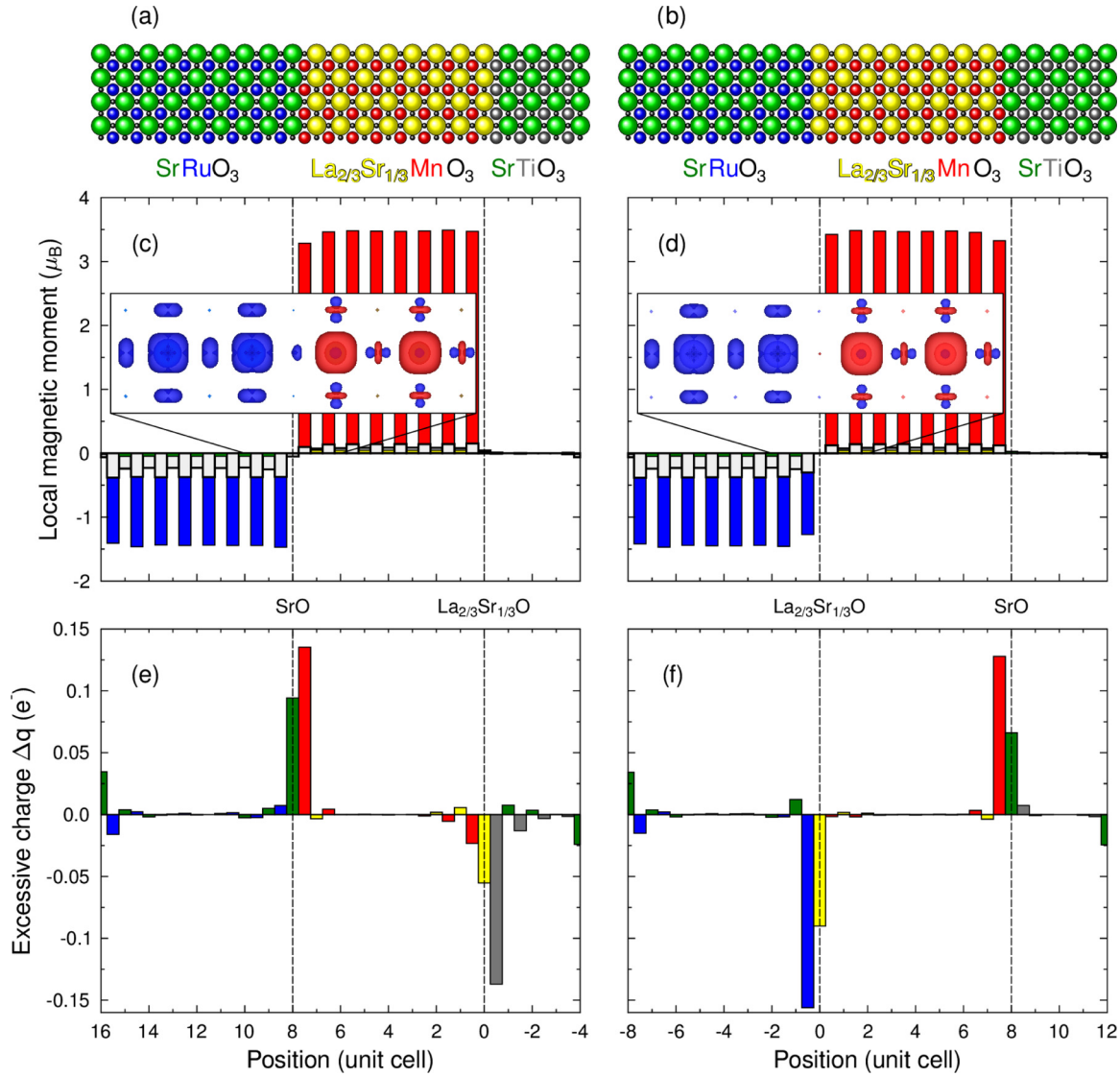

FIG. 5. Density functional theory of layer-resolved magnetic moments, spin densities, and charge transfer at the interface for MnO_2/SrO termination (left) and $RuO_2/La_{0.7}Sr_{0.3}O$ termination (right). (a), (b) Structure model used as a periodic superlattice for calculations. (c), (d) Layer-resolved magnetic moments. Inset: atomically resolved spin density distribution with red/blue denoting spin-up and spin-down densities. Note the higher spin density in (c) at the oxygen ion between Mn and Ru. (e), (f) Interfacial excess charge (in positive elementary charges per atom) for all involved metal ions. Colors agree with (a), (b).

and overcome near –1 T at 60 K. Interface-far parts of the top layers return to the magnetic order of coherently strained (sufficiently thick) single films.

C. Density functional theory

The appearance of an exchange spring in $SrRuO_3$ which is hard magnetic in its bulk form is quite striking and implies the fulfillment of two preconditions: (i) Interfacial Mn-Ru exchange coupling is strong and (ii) interfacial magnetic anisotropy in SRO is low enough. The magnetic coupling at the LSMO-SRO interface has been studied using *ab initio* electronic structure calculations based on density functional theory (described in more detail in the Supplemental Material [30], also see Refs. [39–43]). A Green's function method within a multiple scattering theory has been used for calculating magnetic moments and exchange coupling [39,44]. We consider superlattices consisting of 8 uc of LSMO, 8 uc of SRO, and 4 uc of STO [Figs. 5(a) and 5(b)] in order to account for a potential impact of the STO substrate. In particular, the effect of MnO_2/SrO or $RuO_2/La_{0.7}Sr_{0.3}O$ interface terminations on the strength of exchange coupling has been addressed. (In the periodic superlattice, all interface terminations have been changed accordingly; i.e., only full unit cells of each material appear.) We find that the calculated next-neighbor coupling constant J between Mn and Ru across the interface is larger by a factor of about 3 for the MnO_2/SrO termination (Table I). The value of $J = -13.3$ meV obtained for this interface is even similar in magnitude to the (positive) J value derived for the interior of LSMO. This supports the idea of a rigid Mn-O-Ru coupling at a MnO_2/SrO-terminated interface. Additionally, the difference of the total energy (ΔE) between the states with antiferromagnetic or ferromagnetic coupling of the LSMO and SRO layers across the interface has

TABLE I. Termination-dependent exchange coupling between $La_{0.7}Sr_{0.3}MnO_3$ and $SrRuO_3$ from density functional theory. Difference $\Delta E = E_{AFM} - E_{FM}$ of the total energy for ferromagnetic (E_{FM}) or antiferromagnetic (E_{AFM}) coupling across the interface, and next-neighbor exchange coupling constant J between Mn and Ru.

Termination	ΔE (meV)	J (meV)
MnO_2/SrO	−71.5	−13.3
$RuO_2/La_{0.7}Sr_{0.3}O$	−15.1	−4.5

been determined (Table I). The even fivefold value of ΔE for the MnO_2/SrO termination confirms the much higher stability of the antiferromagnetic coupling for this termination. These results suggest that the antiferromagnetic coupling is considerably stronger for the interface terminated as MnO_2/SrO. Further, the transferred electronic charge at the interfaces has been evaluated [Figs. 5(e) and 5(f)]. The charge transfer does not exceed 0.15 elementary charges for each metal cation (Mn, Ru, Sr, La) at both interfaces and causes weak changes of magnetic moments. On the other hand, our calculation indicates that the spin density at the oxygen ion between Ru and Mn is considerably larger at the MnO_2/SrO-terminated interface than at the $RuO_2/La_{0.7}Sr_{0.3}O$-terminated interface [Figs. 5(c) and 5(d)], pointing towards a plausible origin of the strong coupling. In conclusion, our DFT results suggest a strong impact of the atomic interface termination on the interfacial exchange coupling. In particular, the presence of very strong antiferromagnetic coupling is derived for the MnO_2/SrO-terminated LSMO-SRO interface. It is interesting to emphasize, in the light of these results, that the experimental demonstration of the appearance of two distinct exchange coupling strengths in a LSMO-SRO bilayer by Solignac *et al.* [23] might be related to a coexistence of both interfacial terminations in their sample.

D. STEM

The DFT results have revealed a strong sensitivity of the actual antiferromagnetic coupling strength with respect to the atomic composition of the LSMO-SRO interface. Several of our samples have been investigated by STEM using both mass contrast (HAADF-Z contrast [22]) and EELS for characterizing the interface composition with atomic layer resolution. In HAADF-Z contrast, the intensity at an atomic column grows approximately with the square of the atomic number Z. Since atomic numbers are 38 (Sr) and 51 ($La_{0.7}Sr_{0.3}$) for A site atoms and 25 (Mn) and 44 (Ru) for B site atoms, elemental Z contrast for the LSMO/SRO interface is strong for both A and B sites, allowing one to derive meaningful data for interfacial intermixing from HAADF contrast. We note that interdiffusion occurs only within the same sublattice in the present system because of the strongly different ionic radii at A and B sites. The bulk intensity values of Mn, Ru, Sr, and $La_{0.7}Sr_{0.3}$ columns have been estimated by averaging intensities at atomic positions in a distance of more than 3 uc from the interface (Fig. 6, dashed lines). For SRO grown on LSMO (Fig. 6, left panel), the intensity profile along a

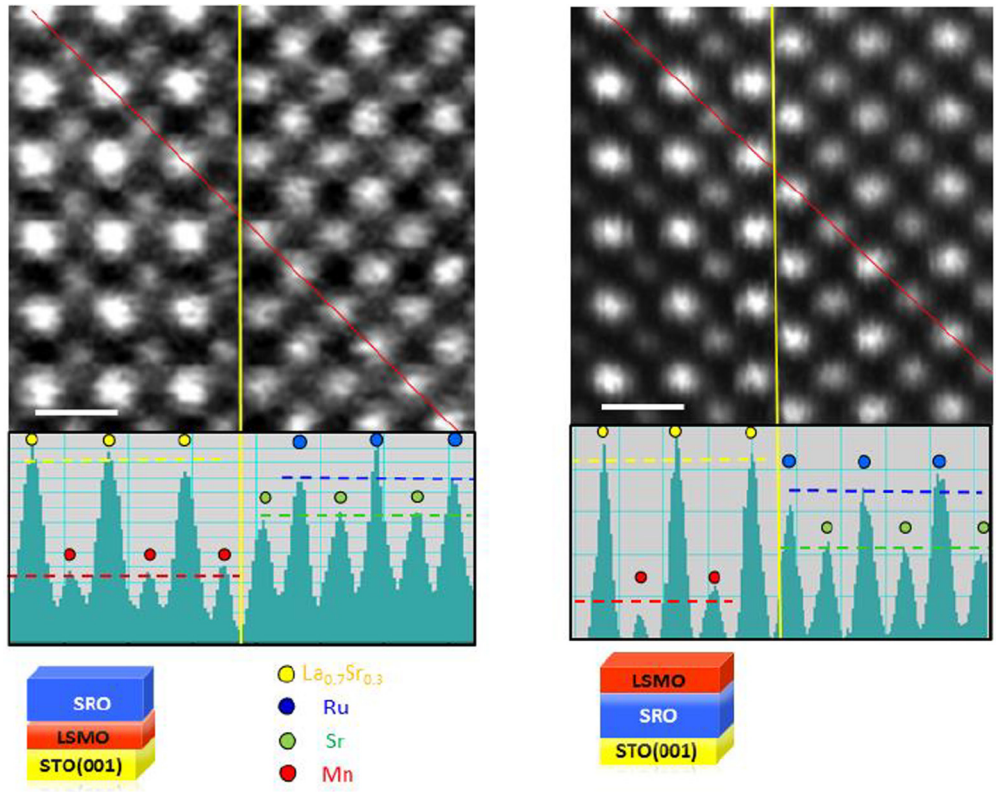

FIG. 6. STEM Z contrast images obtained in high-angle annular dark field (HAADF) mode. The red line in the upper panels marks the position of the line scans shown in the lower panels. Dashed lines indicate averaged interface-far values (explained in the text). The left interface is MnO_2/SrO terminated; the right interface is $RuO_2/La_{0.7}Sr_{0.3}O$ terminated.

line (indicated in red) crossing all types of atomic columns clearly shows a MnO_2-SrO-terminated interface. Mn and Sr intensities at the interface are in agreement with the bulk intensity values within the error range (∼10%). For LSMO on top of SRO (Fig. 6, right panel), a RuO_2-(La,Sr)O interface is clearly visible, even though it shows some moderate interdiffusion. The Mn peak next to the interface is larger than in the bulk, while the Ru site at the interface is slightly reduced in intensity, both indicating some Mn/Ru intermixing. Intermixing at the *A* sites is below the resolution limit in these HAADF images. Averaging over parallel lines crossing the interface in different places confirms the results shown in Fig. 6. Summarizing our HAADF data, they indicate conservation of the *B* site termination from the Ti-terminated substrate to the respective LSMO-SRO interface, with a varying degree of interdiffusion which is low enough not to destroy the type of termination. This implies MnO_2/SrO termination for SRO/LSMO/STO(001) and $RuO_2/La_{0.7}Sr_{0.3}O$ termination for LSMO/SRO/STO(001). We note that the experimentally found $RuO_2/La_{0.7}Sr_{0.3}O$ termination is not expected, since SrO termination has been reported for the surface of SRO/STO(001) films as a result of a termination conversion in the initial growth stage of SRO on STO(001) [45]. In general, the chemical stability of an interface may differ from that of a free surface, and this may even depend on growth conditions. We are aware of a report of a different termination of LSMO/SRO/STO(001) at the LSMO/SRO interface in the work of Yu *et al.* [46]. On the other hand, Ref. [21] finds the same interface terminations as in our work in a $Pr_{0.7}Ca_{0.3}MnO_3$/SRO superlattice.

The $RuO_2/La_{0.7}Sr_{0.3}O$ termination of our bilayers is also confirmed by electron energy loss spectroscopy (EELS) data collected across the interfaces in another sample pair grown at the same growth conditions. Detailed measurements have been performed on the aberration corrected Titan QuantEM microscope of the EMAT laboratory in Antwerp, Belgium; the microscope was operated at 300 kV for imaging and 120 kV for EELS spectroscopy. Figure 7 shows representative element-specific line scans for both sample types obtained from the indicated spectrum images. The composition of atomic planes at the LSMO-SRO interface in the SRO/LSMO/STO(001) sample (upper panel) is as follows: The last MnO_2 plane contains about $25 \pm 5\%$ Ru, and the subsequent SrO plane is rather equally mixed with La like in $Sr_{0.5}La_{0.5}O$. Hence, stronger interdiffusion is notable in this sample than in that one used for the HAADF image where clear MnO_2/SrO termination had been confirmed (Fig. 6). The substrate interface in this sample shows substantial intermixing: The first MnO_2 plane contains around 50% of Ti diffused into the growing film, and Ti is still notable in the second MnO_2 plane. This might be the reason for the stronger intermixing of subsequent interfaces. The composition of atomic planes in the LSMO/SRO/STO(001) sample (lower panel) is as follows. At the interface to the top LSMO layer, Sr and La peaks are very well defined and indicate a low level of *A* site interdiffusion. In the intermediate *B* site plane, Ru dominates and contains around $25 \pm 5\%$ Mn. This confirms the RuO_2 termination for this interface type with moderate Mn admixture. The substrate interface again shows some Ti diffusion into the growing (SRO) film, but it is weaker than in the other bilayer type. Profiles in Figs. 7(c) and 7(f) are the results of two-dimensional (2D) Gaussian fitting of each atomic column intensity averaged line by line over 30 unit cells from a HAADF image taken in the same region as the EELS measurement. These are in perfect agreement with the EELS chemical profile proving that the line-scan EELS measurement is representative of the sample over a large region.

Concluding from the STEM results, our LSMO/SRO/STO(001) bilayers have a dominating $RuO_2/La_{0.7}Sr_{0.3}O$ termination of the LSMO-SRO interface, with varying degree of intermixing depending on sample specifics. This interface termination has been predicted by DFT to show moderate antiferromagnetic coupling. In agreement with that, we observe exchange-bias characteristics and breaking of the interfacial coupling in a field of the order of 1 T (at 60 K, Fig. 4). SRO/LSMO/STO(001) bilayers have a dominating MnO_2/SrO termination of the LSMO-SRO interface, again with a varying degree of intermixing among samples. This interface termination induces a very strong antiferromagnetic coupling according to our DFT results. This agrees with the presence of an exchange spring in this type of bilayer. On the other hand, one expects the actual level of interdiffusion to affect the exchange-spring formation.

IV. FURTHER DISCUSSION AND CONCLUSIONS

Regarding the second precondition for the formation of an exchange spring, the sufficiently low magnetic anisotropy energy, an altered interfacial SRO magnetic anisotropy, must be present. Nonbulklike anisotropy is observed in both respective top layers at the interface with the bottom layer: The SRO top layer shows in-plane interfacial magnetization, whereas the LSMO top layer has canted interfacial Mn moments. The weakening of the interfacial magnetic anisotropy in SRO is likely to be linked to an orthorhombic/tetragonal structural instability of SRO which occurs at a tensile strain of ∼1% [47–49] (not realized here) or as consequence of a volume expansion of 1%–1.5% [50]. Such volume expansion is possible as a result of light cation interdiffusion or an interfacial oxygen vacancy concentration [51]. Alternatively, the transfer of octahedral rotations [10–16] from the bottom into the top layer may be the driving mechanism. To discriminate between these potential mechanisms requires more extended STEM work or an improved general understanding of the interfacial transfer of oxygen octahedral rotations.

For devices of oxide spintronics, the presence of an exchange-spring layer is vitally important. For instance, the exchange-bias function can be completely suppressed, as is obvious in the easy switching of the LSMO soft-magnetic layer coupled to hard-magnetic SRO for the exchange-spring case (Fig. 2). Further, the interfacial spin texture affects electrical transport with regard to electronic spin polarization and effects caused by topologically nontrivial spin arrangements (see below). The reported general features are unlikely to be restricted to the LSMO-SRO interface, since strong exchange coupling may occur at further

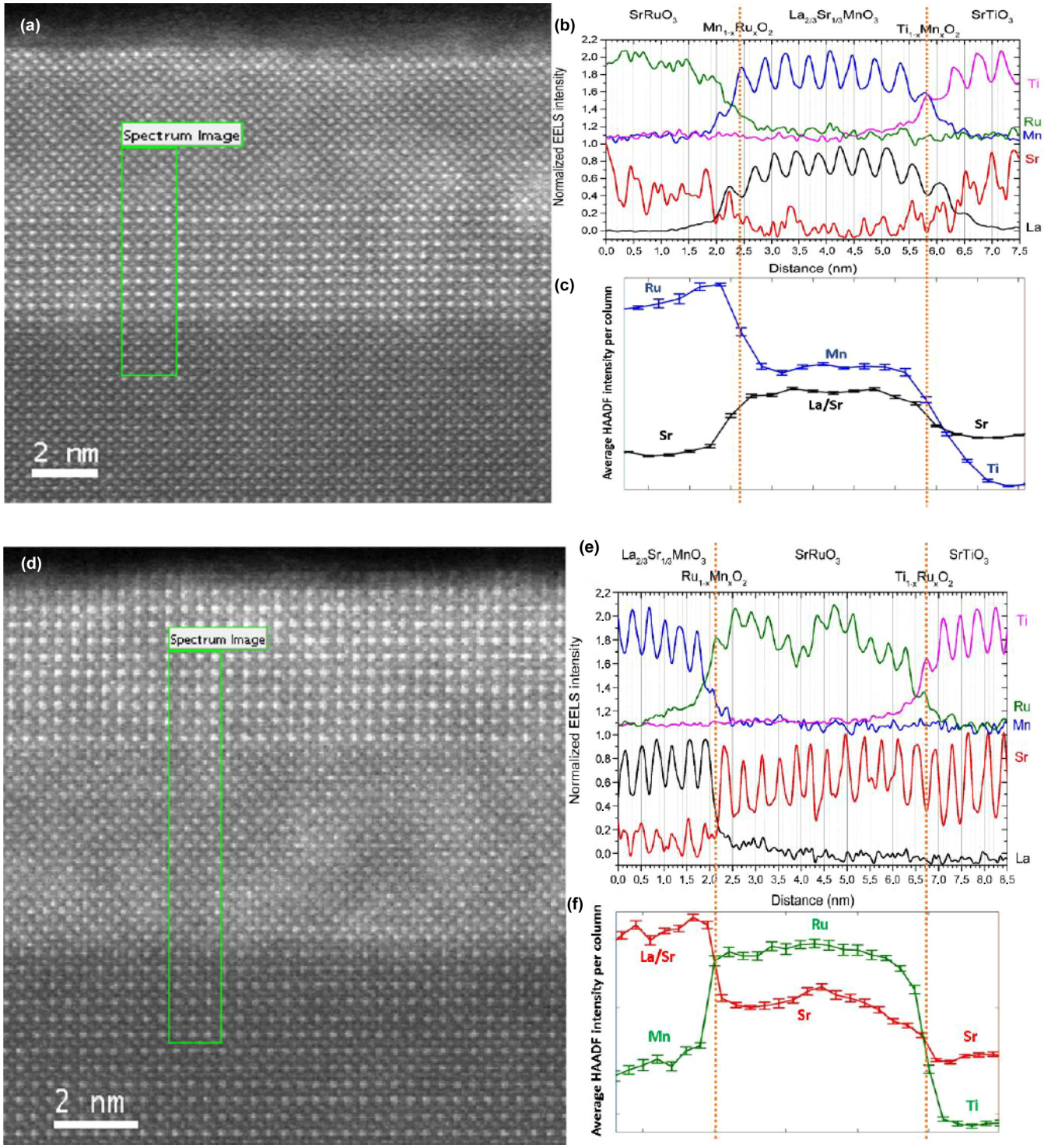

FIG. 7. STEM electron energy loss (EELS) spectroscopy of both interface types. Upper panel: SRO/LSMO/STO(001); lower panel: LSMO/SRO/STO(001). The indicated spectrum image (a), (d) is used to derive the element profiles shown in the right panel (b), (e), respectively. Dashed orange lines mark the interface positions. Panels (c), (f) present the results of a 2D Gaussian fitting of each atomic position over a 30 unit cell region for the *A* site atomic columns (black and red curves) and the *B* site atomic columns (blue and green).

oxide interfaces. Indeed, exchange-spring behavior had already been suggested in $La_{0.7}Sr_{0.3}MnO_3/La_{0.7}Sr_{0.3}CoO_3$ [52] and $Fe_3O_4/CoFe_2O_4$ [53]. On the other hand, noncollinear interfacial spin textures are highly promising for spintronics functionalities. For the studied system with a SRO top layer, a spin valve can be envisaged where a magnetic field of a few mT can set the SRO spin texture into four different states, exploiting the biaxial in-plane easy axes of LSMO and the large switching field of the hard-magnetic top SRO part. Such a device can serve for fundamental investigations of the electron transport through switchable noncollinear spin textures in strongly correlated electron systems.

Some of the resulting Ru spin textures are noncoplanar and thus have nonvanishing scalar spin chirality [54]. Hence, a topological Hall effect is expected to occur. In agreement with this expectation, a recent report on the Hall effect of LSMO-SRO bilayers shows features tentatively attributed to the THE [27]. In the future, understanding and manipulating interfacial spin textures in oxides offers tremendous potential for designing domain walls and magnetic skyrmions like in metallic heterostructures [1,2], but with the additional control parameters offered by complex oxides (like electric-field control for lower energy consumption) and faster operation.

ACKNOWLEDGMENTS

The research in Halle was supported by Deutsche Forschungsgemeinschaft (DFG), SFB 762 Functional Oxide Interfaces (Projects No. A9 and No. B1). K.C. benefited from support of the DFG (Project 600575). Discussions with M. Trassin, M. Ziese, H. M. Christen, E.-J. Guo, F. Grcondciel, M. Bibes, and H. N. Lee are gratefully acknowledged. N.G. and J.V. acknowledge funding under the GOA project "Solarpaint" of the University of Antwerp. The Qu-Ant-EM microscope was partly funded by the Hercules fund from the Flemish Government.

[1] A. Fert, V. Cros, and J. Sampaio, Skyrmions on the track, Nat. Nanotechnol. **8**, 152 (2013).

[2] G. Chen and A. K. Schmid, Imaging and tailoring the chirality of domain walls in magnetic films, Adv. Mater. **27**, 5738 (2015).

[3] F. Y. Bruno *et al.*, Insight into spin transport in oxide heterostructures from interface-resolved magnetic mapping, Nat. Commun. **6**, 6306 (2015).

[4] P. Xu *et al.*, Reversible formation of 2D electron gas at the $LaFeO_3/SrTiO_3$ interface via control of oxygen vacancies, Adv. Mater. **29**, 1604447 (2017).

[5] P. Yu, J. S. Lee, S. Okamoto, M. D. Rossell, M. Huijben, C. H. Yang, Q. He, J. X. Zhang, S. Y. Yang, M. J. Lee, Q. M. Ramasse, R. Erni, Y. H. Chu, D. A. Arena, C. C. Kao, L. W. Martin, and R. Ramesh, Interface Ferromagnetism and Orbital Reconstruction in $BiFeO_3$-$La_{0.7}Sr_{0.3}MnO_3$ Heterostructures, Phys. Rev. Lett. **105**, 027201 (2010).

[6] B.-C. Huang, P. Yu, Y. H. Chu, C.-S. Chang, R. Ramesh, R. E. Dunin-Borkowski, P. Ebert, and Y.-P. Chiu, Atomically resolved electronic states and correlated magnetic order at termination engineered complex oxide heterointerfaces, ACS Nano **12**, 1089 (2018).

[7] E.-J. Guo *et al.*, Spatially resolved large magnetization in ultrathin $BiFeO_3$, Adv. Mater. **29**, 1700790 (2017).

[8] J. Matsuno, N. Ogawa, K. Yasuda, F. Kagawa, W. Koshibae, N. Nagaosa,Y. Tokura, and M. Kawasaki, Interface-driven topological Hall effect in$SrRuO_3$-SrIrO3 bilayer, Sci. Adv. **2**, e1600304 (2016).

[9] Y. Ohuchi1, J. Matsuno, N. Ogawa, Y. Kozuka, M. Uchida, Y. Tokura, and M. Kawasaki, Electric-field control of anomalous and topological Hall effects in oxide bilayer thin films, Nat. Commun. **9**, 213 (2018).

[10] E. J. Moon, R. Colby, Q. Wang, E. Karapetrova, C. M. Schlepütz, M. R. Fitzsimmons, and S. J. May, Spatial control of functional properties via octahedral modulations in complex oxide superlattices, Nat. Commun. **5**, 5710 (2014).

[11] E. J. Moon, P. V. Balachandran, B. J. Kirby, D. J. Keavney, R. J. Sichel-Tissot, C. M. Schlepütz, E. Karapetrova, X. M. Cheng, J. M. Rondinelli, and S. J. May, Effect of interfacial octahedral behavior in ultrathin manganite films, Nano Lett. **14**, 2509 (2014).

[12] J. Chakhalian, J. W. Freeland, A. J. Millis, C. Panagopoulos, and J. M. Rondinelli, Emergent properties in plane view: Strong correlations at oxide interfaces, Rev. Mod. Phys. **86**, 1189 (2014).

[13] Q. He, R. Ishikawa, A. R. Lupini, L. Qiao, E. J. Moon, O. Ovchinnikov, S. J. May, M. D. Biegalski, and A. Y. Borisevich, Towards 3D mapping of BO_6 octahedron rotations at perovskite heterointerfaces, unit cell by unit cell, ACS Nano **9**, 8412 (2015).

[14] D. Kan, R. Aso, R. Sato, M. Haruta, H. Kurata, and Y. Shimakawa, Tuning magnetic anisotropy by interfacially engineering the oxygen coordination environment in a transition metal oxide, Nat. Mater. **15**, 432 (2016).

[15] Z. Liao *et al.*, Controlled lateral anisotropy in correlated manganite heterostructures by interface-engineered oxygen octahedral coupling, Nat. Mater. **15**, 425 (2016).

[16] Z. Liao *et al.*, Thickness dependent properties in oxide heterostructures driven by structurally induced metal–oxygen hybridization variations, Adv. Func. Mater. **27**, 1606717 (2017).

[17] X. Ke, M. S. Rzchowski, L. J. Belenky, and C. B. Eom, Positive exchange bias in ferromagnetic $La_{0.67}Sr_{0.33}MnO_3/SrRuO_3$ bilayers, Appl. Phys. Lett. **84**, 5458 (2004).

[18] M. Ziese, I. Vrejoiu, E. Pippel, P. Esquinazi, D. Hesse, C. Etz, J. Henk, A. Ernst, I. V. Maznichenko, W. Hergert, and I. Mertig, Tailoring Magnetic Interlayer Coupling in $La_{0.7}Sr_{0.3}MnO_3/SrRuO_3$ Superlattices, Phys. Rev. Lett. **104**, 167203 (2010).

[19] J. W. Seo, W. Prellier, P. Padhan, P. Boullay, J. Y. Kim, H. Lee, C. D. Batista, I. Martin, E. E. M. Chia, T. Wu, B. G. Cho, and C. Panagopoulos, Tunable Magnetic Interaction at the Atomic Scale in Oxide Heterostructures, Phys. Rev. Lett. **105**, 167206 (2010).

[20] M. Ziese, I. Vrejoiu, E. Pippel, E. Nikulina, and D. Hesse, Magnetic properties of $Pr_{0.7}Ca_{0.3}MnO_3/SrRuO_3$ superlattices, Appl. Phys. Lett. **98**, 132504 (2011).

[21] M. Ziese, I. Vrejoiu, E. Pippel, A. Hähnel, E. Nikulina, and D. Hesse, Orthorhombic-to-tetragonal transition of $SrRuO_3$ layers in $Pr_{0.7}Ca_{0.3}MnO_3/SrRuO_3$ superlattices, J. Phys. D **44**, 345001 (2011).

[22] R. Hillebrand, E. Pippel, D. Hesse, and I. Vrejoiu, A study of intermixing in perovskite superlattices by simulation-supported C_s-corrected HAADF-STEM, Phys. Status Solidi A **208**, 2144 (2011).

[23] A. Solignac, R. Guerrero, P. Gogol, T. Maroutian, F. Ott, L. Largeau, P. Lecoeur, and M. Pannetier-Lecoeur, Dual Antiferromagnetic Coupling at $La_{0.67}Sr_{0.33}MnO_3/SrRuO_3$ Interfaces, Phys. Rev. Lett. **109**, 027201 (2012).

[24] J. H. Kim, I. Vrejoiu, Y. Khaydukov, T. Keller, J. Stahn, A. Ruhm, D. K. Satapathy, V. Hinkov, and B. Keimer,

Competing interactions at the interface between ferromagnetic oxides revealed by spin-polarized neutron reflectometry, Phys. Rev. B **86**, 180402(R) (2012).

[25] X. Ke, L. J. Belenky, V. Lauter, H. Ambaye, C. W. Bark, C. B. Eom, and M. S. Rzchowski, Spin Structure in an Interfacially Coupled Epitaxial Ferromagnetic Oxide Heterostructure, Phys. Rev. Lett. **110**, 237201 (2013).

[26] S. Das, A. Herklotz, E. Pippel, E. J. Guo, D. Rata, and K. Dörr, Strain dependence of antiferromagnetic interface coupling in$La_{0.7}Sr_{0.3}MnO_3/SrRuO_3$superlattices, Phys. Rev. B **91**, 134405 (2015).

[27] I. Lindfors-Vrejoiu and M. Ziese, Topological Hall effect in antiferromagnetically coupled$SrRuO_3/La_{0.7}Sr_{0.3}MnO_3$epitaxial heterostructures, Phys. Status Solidi B **254** (2017).

[28] S. Agrestini, Z. Hu, C. Y. Kuo, M. W. Haverkort, K. T. Ko, N. Hollmann, Q. Liu, E. Pellegrin, M. Valvidares, Herrero-J. Martin, P. Gargiani, P. Gegenwart, M. Schneider, S. Esser, A. Tanaka, A. C. Komarek, and L. H. Tjeng, Electronic and spin states of $SrRuO_3$ thin films: An x-ray magnetic circular dichroism study, Phys. Rev. B **91**, 075127 (2015).

[29] Y. Jia, R. V. Chopdekar, E. Arenholz, Z. Liu, M. D. Biegalski, Z. D. Porter, A. Mehta, and Y. Takamura, Thickness dependence of exchange coupling in (111)-oriented perovskite oxide superlattices, Phys. Rev. B **93**, 104403 (2016).

[30] See Supplemental Material at http://link.aps.org/supplemental/10.1103/PhysRevB.99.024416 for more information regarding details on sample growth and density functional theory.

[31] J. Choi and C. B. Eom, Growth mode transition from layer by layer to step flow during the growth of heteroepitaxial$SrRuO_3$on (001) $SrTiO_3$, Appl. Phys. Lett. **79**, 1447 (2001).

[32] G. Rijnders and D. H. A. Blank, Enhanced surface diffusion through termination conversion during epitaxial$SrRuO_3$growth, Appl. Phys. Lett. **84**, 505 (2004).

[33] E. F. Kneller and R. Hawig, The exchange-spring magnet: A new material principle for permanent magnets, IEEE Trans. Magn. **27**, 3588 (1991).

[34] Y. Choi, J. S. Jiang, J. E. Pearson, S. D. Bader, J. J. Kavich, J. W. Freeland, and J. P. Liu, Controlled interface profile in Sm–Co/Fe exchange-spring magnets, Appl. Phys. Lett. **91**, 072509 (2007).

[35] A. Berger, N. Supper, Y. Ikeda, B. Lengsfield, A. Moser, and E. E. Fullerton, Improved media performance in optimally coupled exchange spring layer media, Appl. Phys. Lett. **93**, 122502 (2008).

[36] M. Huijben, L. W. Martin, Y. H. Chu, M. B. Holcomb, P. Yu, G. Rijnders, D. H. A. Blank, and R. Ramesh, Critical thickness and orbital ordering in ultrathin$La_{0.7}Sr_{0.3}MnO_3$films, Phys. Rev. B **78**, 094413 (2008).

[37] M. Ziese, Magnetocrystalline anisotropy transition in $La_{0.7}Sr_{0.3}MnO_3$ films, Phys. Status Solidi B **242**, R116 (2015).

[38] M. Ziese, I. Vrejoiu, and D. Hesse, Structural symmetry and magnetocrystalline anisotropy of$SrRuO_3$films on $SrTiO_3$, Phys. Rev. B **81**, 184418 (2010).

[39] M. Geilhufe, S. Achilles, M. A. Köbis, M. Arnold, I. Mertig, W. Hergert, and A. Ernst, Numerical solution of the relativistic single-site scattering problem for the Coulomb and the Mathieu potential, J. Phys.: Condens. Matter **27**, 435202 (2015).

[40] C. Etz, I. V. Maznichenko, D. Bottcher, J. Henk, A. N. Yaresko, W. Hergert, I. I. Mazin, I. Mertig, and A. Ernst, Indications of weak electronic correlations in$SrRuO_3$from first-principles calculations, Phys. Rev. B **86**, 064441 (2012).

[41] V. I. Anisimov, J. Zaanen, and O. K. Andersen, Band theory and Mott insulators: Hubbard *U* instead of Stoner *I*, Phys. Rev. B **44**, 943 (1991).

[42] L. Uba, S. Uba, L. P. Germash, L. V. Bekenov, and V. N. Antonov, Electronic structure and magneto-optical spectra of $La_xSr_{1-x}MnO_3$ perovskites: Theory and experiment. Phys. Rev. B **85**, 125124 (2012).

[43] B. L. Gyorffy, Coherent-potential approximation for a non-overlapping muffin-tin-potential model of random substitutional alloys, Phys. Rev. B **5**, 2382 (1972).

[44] M. Luders, A. Ernst, M. Dane, Z. Szotek, A. Svane, D. Kodderitzsch, W. Hergert, B. L. Gyorffy, and W. M. Temmerman, Self-interaction correction in multiple scattering theory, Phys. Rev. B **71**, 205109 (2005).

[45] G. Koster, L. Klein, W. Siemons, G. Rijnders, J. S. Dodge, C.-B. Eom, D. H. A. Blank, and M. R. Beasley, Structure, physical properties, and applications of$SrRuO_3$thin films, Rev. Mod. Phys. **84**, 253 (2012).

[46] P. Yu, W. Luo, D. Yi, J. X. Zhang, M. D. Rossell, C.-H. Yang, L. You, G. Singh-Bhalla, S. Y. Yang, Q. He, Q. M. Ramasse, R. Erni, L. W. Martin, Y. H. Chu, S. T. Pantelides, S. J. Pennycook, and R. Ramesh, Interface control of bulk ferroelectric polarization, Proc. Natl. Acad. Sci. USA **109**, 9710 (2012).

[47] A. Vailionis, W. Siemons, and G. Koster, Room temperature epitaxial stabilization of a tetragonal phase in $ARuO_3$ (A = Ca and Sr) thin films, Appl. Phys. Lett. **93**, 051909 (2008).

[48] A. Herklotz, M. Kataja, K. Nenkov, M. D. Biegalski, H. M. Christen, C. Deneke, L. Schultz, and K. Dörr, Magnetism of the tensile-strain-induced tetragonal state of$SrRuO_3$films, Phys. Rev. B **88**, 144412 (2013).

[49] A. Herklotz and K. Dörr, Characterization of tetragonal phases of $SrRuO_3$ under epitaxial strain by density functional theory, Eur. Phys. J. B **88**, 60 (2015).

[50] A. Herklotz, A. T. Wong, T. Meyer, M. D. Biegalski, H. N. Lee, and T. Z. Ward, Controlling octahedral rotations in a perovskite via strain doping, Sci. Rep. **6**, 26491 (2016).

[51] A. Y. Borisevich, A. R. Lupini, J. He, E. A. Eliseev, A. N. Morozovska, G. S. Svechnikov, P. Yu, Y. H. Chu, R. Ramesh, S. T. Pantelides, S. V. Kalinin, and S. J. Pennycook, Interface dipole between two metallic oxides caused by localized oxygen vacancies, Phys. Rev. B **86**, 140102(R) (2012).

[52] B. Li, R. V. Chopdekar, E. Arenholz, A. Mehta, and Y. Takamura, Unconventional switching behavior in $La_{0.7}Sr_{0.3}MnO_3/La_{0.7}Sr_{0.3}CoO_3$ exchange spring bilayers, Appl. Phys. Lett. **105**, 202401 (2014).

[53] A. V. Ramos, J. B. Moussy, M. J. Guittet, Gautier-M. Soyer, C. Gatel, Bayle-P. Guillemaud, Warot-B. Fonrose, and E. Snoeck, Influence of a metallic or oxide top layer in epitaxial magnetic bilayers containing $CoFe_2O_4$(111) tunnel barriers, Phys. Rev. B **75**, 224421 (2007).

[54] N. Nagaosa, X. Z. Yu, and Y. Tokura, Gauge fields in real and momentum spaces in magnets: Monopoles and skyrmions, Philos. Trans. R. Soc., A **370**, 5806 (2012).